THE JOURNAL OF PHYSICAL CHEMISTRY LETTERS
A JOURNAL OF THE AMERICAN CHEMICAL SOCIETY
pubs.acs.org/JPCL
Letter

Molecular Dynamics Study of the Photodegradation of Polymeric Chains

Meade Erickson, Yulun Han, Bakhtiyor Rasulev,* and Dmitri Kilin*

Cite This: *J. Phys. Chem. Lett.* 2022, 13, 4374−4380
Read Online

ABSTRACT: The development of reusable polymeric materials inspires an attempt to combine renewable biomass with upcycling to form a biorenewable closed system. It has been reported that 2,5-furandicarboxylic acid (FDCA) can be recovered for recycling when incorporated as monomers into photodegradable polymeric systems. Here, we conduct density functional theory (DFT) studies with periodic boundary conditions on microscopic structures involved in the photodegradation of polymeric chains incorporating FDCA and 2-nitro-1,3-benzenedimethanol. The photodegradation process of polymeric chains is studied using time-dependent excited-state molecular dynamics (TDESMD) in vacuum and aqueous environments. Changes in the photophysical properties for reaction intermediates are characterized by ground-state observables. The distribution of reaction intermediates and products is obtained from TDESMD trajectories using cheminformatics techniques. Results show that a higher degree of polymeric chain degradation is achieved in the vacuum environment. Additionally, one finds that the FDCA molecule is recoverable in the aqueous environment, in qualitative agreement with experimental findings.

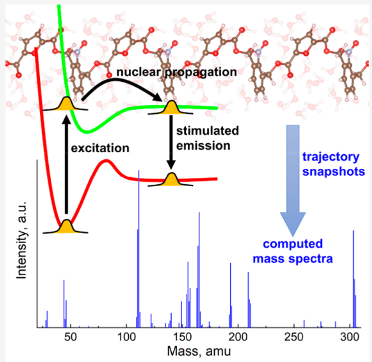

Pressure has grown for industrial members to produce chemicals and materials following green chemistry guidelines due to increasing environmental impacts, public interest, and regulatory policies.[1] One strategy is upcycling[2] with the closed-loop methodology to recycle materials and prevent them being disposed into waste facilities. Biomass, specifically fructose, has been highlighted as a carbon source replacement of fossil fuels due to its availability, extensive opportunities for development of chemical compounds, and reusability.[3,4] To further comply with green chemistry principles, one can combine renewable biomass with upcycling to form a biorenewable closed system for the development of recoverable and reusable materials with reducing reliance on fossil fuels. Previously, experimental studies have shown that 2,5-furandicarboxylic acid (FDCA) can be recovered for recycling when incorporated as building blocks into photodegradable polymeric systems.[5] Briefly, the experiment proceeds with the generation of FDCA from fructose, which then reacts with 2-nitro-1,3-benzenedimethanol that has photocleavable functionality (i.e., phototrigger) to form polymeric/oligomeric compounds. Photodegradation of such polymeric/oligomeric compounds under UV light leads to the photocleavage of the polymeric material, as well as the recovery of FDCA monomers. This strategy has the potential to build plastics that are synthetic or biobased, recyclable, and photodegradable in natural environments. To realize its full potential, it is necessary to conduct detailed studies on the mechanism and related sequence of reaction steps and microscopic structures involved in the photodegradation.

A number of computational methods have been applied to investigate the degradation pathways of polymeric systems such as reactive force field (ReaxFF)[6,7] and transition state theory.[8] Density functional theory (DFT) based *ab initio* molecular dynamics (AIMD) is widely used to simulate reaction processes while maintaining a reasonable computational expense, providing opportunities for the exploration of microscopic information that is inaccessible from experimental data, elucidation of reaction mechanisms, and development of predictive models for further research.[9−14] To model photo-induced reactions, one needs to go beyond Born−Oppenheimer approximation and account for nonadiabatic transition between manifolds of electronic states. One such method is nonadiabatic molecular dynamics (NAMD)[15−20] using Tully's surface hopping,[21] which has been used to study photoreaction of organic molecules[22] and conjugated oligomers.[23] Our group has developed a DFT-based time-dependent excited-state molecular dynamics (TDESMD)[24,25] algorithm, the implementation of which rests on the combination of Rabi theory[26,27] and surface hopping approximation.[21] In the TDESMD algorithm, a molecule experiences cyclic excitations and de-excitations between the ground state and excited state

Received: March 18, 2022
Accepted: May 4, 2022
Published: May 11, 2022

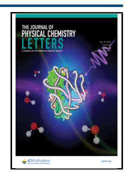

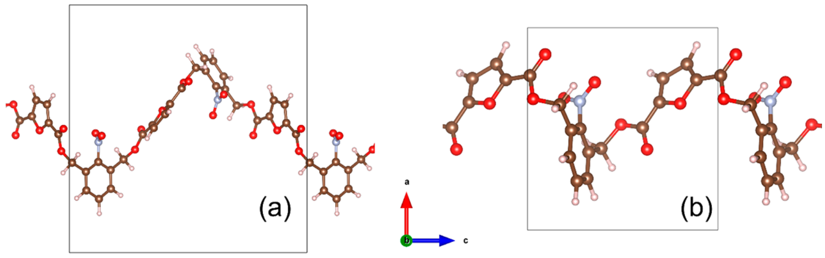

Figure 1. Views of geometry-optimized structures in (a) vacuum and (b) aqueous environments. The box represents the simulation cell used in the simulation. In panel (b), the free water molecules are not shown for clarity. White, red, brown, and blue spheres represent H, O, C, and N atoms, respectively.

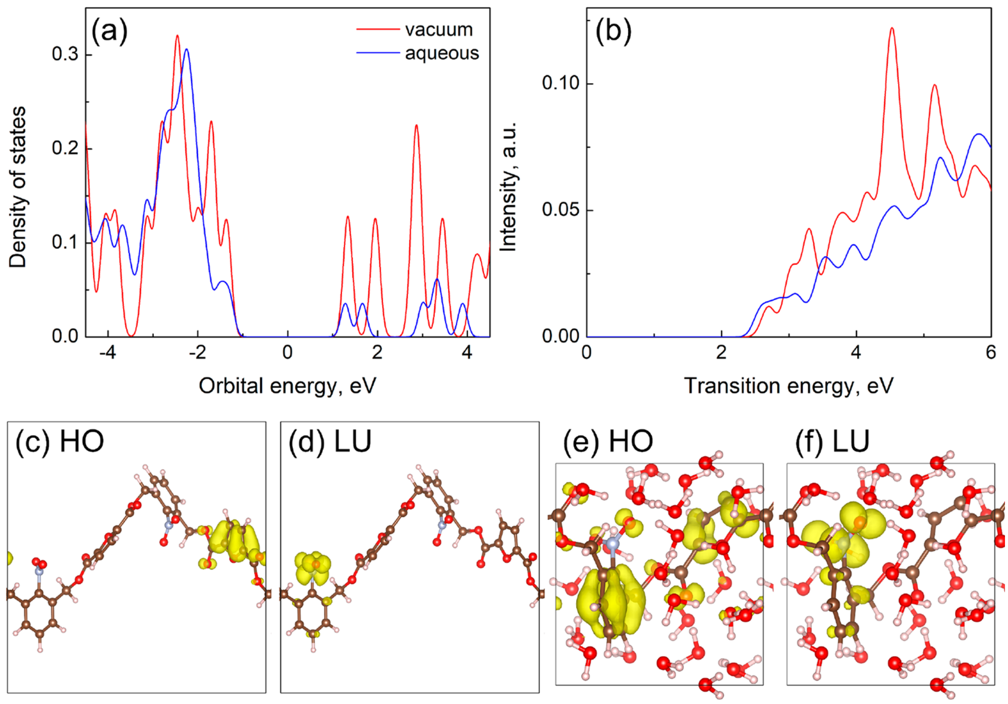

Figure 2. (a) DOS, (b) calculated absorption spectra, and (c−f) partial charge densities for frontier orbitals of optimized structures in vacuum and aqueous environments.

to model the perturbation of molecules by light. The TDESMD method has been used to explore photoreactions for a range of materials.[24,25,28−31] In this work, we carry out TDESMD calculations on polymeric chains consisting of biobased FDCA and nitrobenzyl chromophore to gain a better understanding of the photodegradation and possible ways to control basic processes that allow the deconstruction of the polymers and recycling of the monomers. The deconstruction will turn the polymer into individual building blocks, ready for repolymerization, thus implementing a concept of polymer upcycling using bioderived materials.

The TDESMD algorithm is briefly described in Supporting Information. The extended details have been documented eslewhere.[25,32] Practical calculations are performed in a basis set of Kohn−Sham (KS) orbitals computed in DFT using the Perdew−Burke−Ernzerhof (PBE)[33] form of generalized gradient approximation (GGA),[34,35] with the projected augmented wave (PAW)[36] potentials as implemented in the Vienna *ab initio* simulation package (VASP).[37−41] The long-range internuclear interactions are treated with the semi-empirical pairwise corrections DFT-D3.[42] The distribution of reaction intermediates and products along TDESMD trajectories is obtained using cheminformatics tools such as Open Babel.[43] Ground-state observables such as density of states (DOS), partial charge density, and absorption spectra are obtained from geometry-optimized models. The geometry-optimized models also serve as starting points for TDESMD calculations. We consider two polymeric chains under periodic boundary conditions, corresponding to two environment media; see Figure 1. In the vacuum phase, each periodically replicated simulation cell contains two FDCA-nitrobenzyl units ($C_{28}H_{18}N_2O_{14}$). In the aqueous phase, the simulation cell contains one FDCA-nitrobenzyl unit ($C_{14}H_9N_1O_7$) surrounded by 27 H_2O molecules.

Figure 2 shows ground-state electronic properties for geometry-optimized models in vacuum and aqueous environments. In the DOS, the orbital energy is reported with respect to Fermi energy, which is defined as the midpoint between the HO (highest occupied molecular orbital) and LU (lowest unoccupied molecular orbital). The presence of water does not induce drastic changes to symmetry and energy for orbitals near the band gap. The number of orbitals of the same symmetry on the model structure in the vacuum phase is about two times larger than in the aqueous phase, due to the different

https://doi.org/10.1021/acs.jpclett.2c00802
J. Phys. Chem. Lett. 2022, 13, 4374−4380

number of polymeric units per simulation cell. The charge density is mainly localized on the nitro group for HO-3/HO-2/LU/LU+1 in a vacuum and for HO-1/LU in the aqueous phase. In contrast, the charge density is concentrated on the furan group for HO-1/HO/LU+2/LU+3 in the vacuum phase and for LU+1 in the aqueous phase. Delocalization of charge density over both furan and nitrobenzyl groups is observed for HO-5/HO-4/LU+4/LU+5 in the vacuum phase and for HO-2/HO/LU+2/LU+4/LU+5 in the aqueous phase.

The absorption spectra for geometry-optimized models in vacuum and aqueous environments are calculated using independent orbital approximations (IOAs).[44,45] The intensities of HO → LU transitions are low since the orbital overlap is not strong. The atomistic model in the aqueous phase shows lower absorption than in the vacuum phase since the presence of polar water molecules affects the shape of orbitals and reduces the oscillator strengths and transition dipoles for discernible transitions. The intense transitions have high oscillator strengths, which are the more probable to take place. Thus, they are used as the initial transitions for TDESMD calculations. In what follows, we focus on the TDESMD trajectories induced by the intense transitions HO → LU+3 (~3.3 eV) in the vacuum phase with localized charge densities on the furan group and HO-2 → LU+2 (~4.6 eV) in the aqueous phase with delocalized charge densities over the furan and phenyl rings.

In TDESMD calculations, one explores the ground- and excited-state potential energy surfaces. The implementation of Rabi oscillations that highlights the role of electron transitions will facilitate the accumulation of kinetic energy leading to vivid reactions by overcoming the dissociation barrier. Figure 3 shows the representative snapshots focusing on the generation of FDCA along the TDESMD trajectory in the vacuum phase. Snapshots highlight the major reaction intermediates and products. The reaction events are rare for the initial stage of the trajectory, as the accumulated kinetic energy is low. Later in the trajectory, one observes bond breaking of C−O between the acyl group and oxygen. From ~1165 to 1720 fs, one observes the sequential cleavage of C−O bonds in alkoxyl groups. The cleavage converts the polymeric chain into separate fragments. Meanwhile, one nitro group is found to be labile. One observes excessive rotation and bond stretching between the nitrogen of the NO_2 group and the carbon of the phenyl ring. At 1720 fs, one finds the formation of two CO_2 fragments as a result of C−C bond breaking in dehydrogenated FDCA fragments. The remaining furan groups break apart to form high stretching furan derivatives. Both furan derivatives contain at least one oxygen from ester. Subsequently, a third CO_2 fragment is formed, which is then recaptured by the benzene derivatives. The further fragmentation leads to the CO group attached to the terminal CH_2 of the benzene derivatives and O attached to the furan derivative. In final stages, this benzene derivative undergoes ring expansion, which generates a cycloheptane ring. The CO group is ejected to produce a CO fragment.

Figure 4 shows the representative snapshots focusing on the generation of FDCA along the TDESMD trajectory in the aqueous phase. Similar to the trajectory in the vacuum phase, the reaction events are rare in the initial stages due to an insufficient amount of thermal energy. Note that the reaction steps shown in the aqueous phase trajectory follow the qualitative trend of photodegradation processes in experimental work of the 2-nitrobenzyl chromophore.[46−48] At ~1265 fs, one observes the first cleavage of the C−O bond in one of the alkoxyl groups. At ~1350 fs, the remaining C−O bond in the alkoxyl group is also cleaved, leading to a standalone $FDCA^{2-}$ anion and dicarbonium ion $(C_6H_3NO_2)(CH_2)_2^{2+}$. Note that this C−O bond experiences several cycles of forming and breaking in the later trajectory. Meanwhile, there are frequent proton transfer events among water molecules. At ~1400 fs, a hydroxide ion is captured by one carbonium ion, which is later converted into a formyl group by subsequent proton transfer to surrounding water molecules. At ~1500 fs, proton transfer from a neighboring water molecule to carboxylate group leads to a carboxyl group in the $FDCA^-$ ion. Proton transfer events involving water and FDCA fragment become abundant for the rest of the trajectory due to increased thermal energy. At ~1700 fs, proton transfer occurs in the nitro group, which is later converted into a nitroso group. The C−N bond rotation is seen before and during the interaction of the water H and O of the nitro group. At ~2100 fs, a hydroxide ion interacts with the phenyl ring, resulting in a sp^3-hybridized carbon. Thus, the phenyl ring changes from planar orientation into a nonrigid nonplanar orientation. At later stages, the H atom originally bound to sp^3-carbon is ejected and is captured by the carboxylate group leading to an intact FDCA molecule at 2230 fs of the trajectory. The formation of the intact FDCA molecule agrees with experimental findings highlighting the recovery of FDCA after photoirradiation.[5] A representative chemical scheme from an initial polymer to the product in the aqueous phase is shown in Supporting Information (Scheme S1).

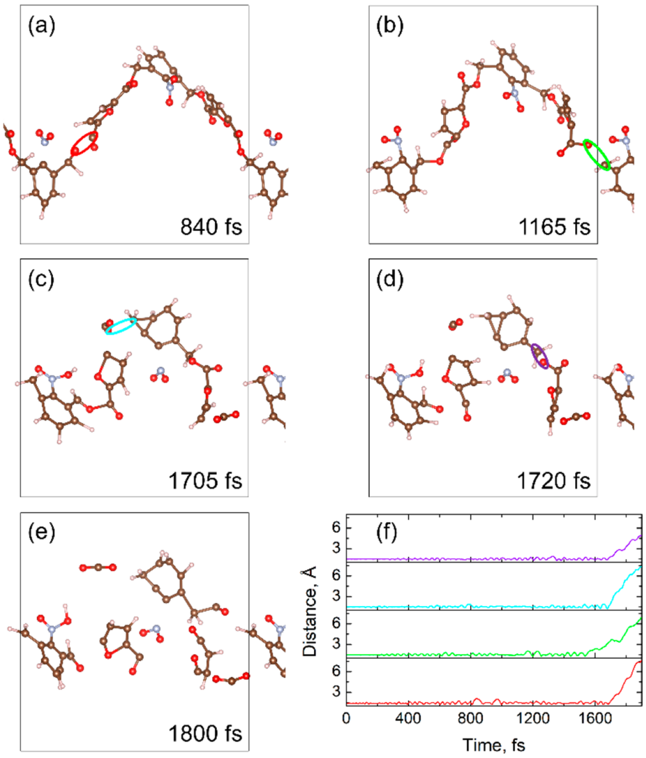

Figure 3. (a−e) Representative snapshots along the TDESMD trajectory with electron hopping between the orbital pair (HO, LU+3) for the atomistic model in the vacuum phase. (f) Time dependence of interatomic C−O distances during the trajectory. The involved atomic pair is highlighted in panels (a−d) with the same color scheme.

https://doi.org/10.1021/acs.jpclett.2c00802
J. Phys. Chem. Lett. 2022, 13, 4374−4380

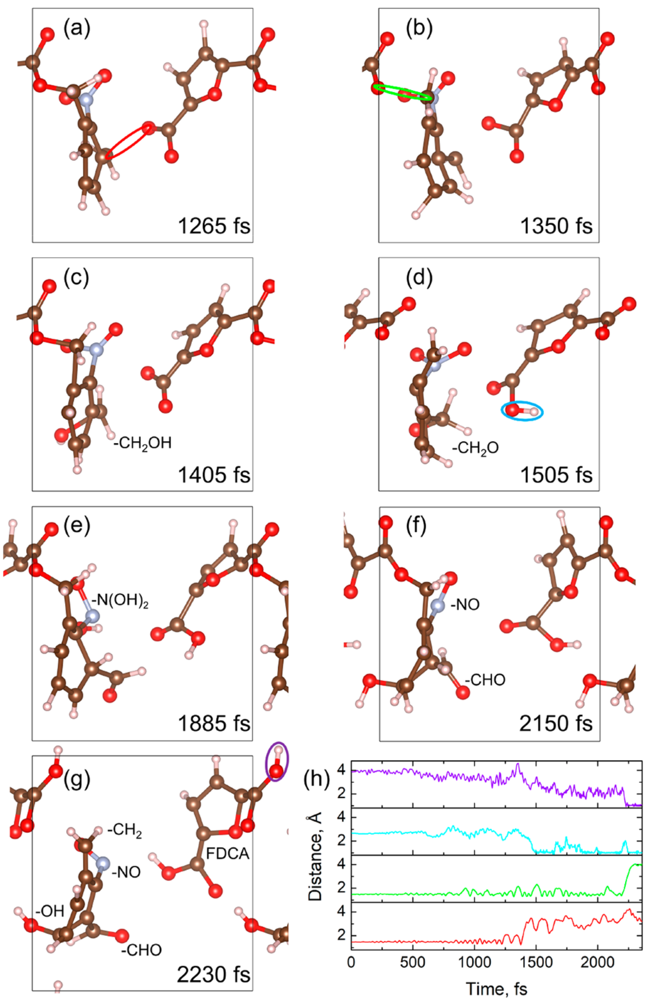

Figure 4. (a−g) Representative snapshots along the TDESMD trajectory with electron hopping between the orbital pair (HO-2, LU+2) for the atomistic model in the aqueous phase. (h) Time dependence of interatomic C−O (red and green) and O−H (cyan and purple) distances during the trajectory. The involved atomic pair is highlighted in panels (a−g) with the same color scheme.

There are notable differences between TDESMD trajectories in vacuum and aqueous environments. Specifically, decomposition of polymeric chain in the vacuum phase occurs at earlier stages than the aqueous phase. The degree of decomposition is greater in the vacuum phase than the aqueous phase. Additionally, the intact FDCA molecule is formed in the aqueous phase, while in the vacuum only dehydrogenated FDCA fragment is present.

Figure 5 shows the distribution of reaction intermediates and products along TDESMD trajectories in vacuum and aqueous environments. Here, we focus on species with a molecular weight less than one unit of FDCA-nitrobenzyl compound. The higher intensity of a peak in the spectra suggests the longer period of time that a specific fragment is present in the trajectory. As the trajectory proceeds forward, smaller backbone fragments with lighter molecular weights are formed. In the low mass region of both spectra, the closed-shell molecules such as NO_2, CO_2, and CO are clearly observed. In the high mass region, labels 1−6 (in the vacuum phase) and 1′-6′ (in the aqueous phase) indicate abundant fragments with varying structures starting from the highest molecular weight to the lowest. Within each labeled groups, there are several

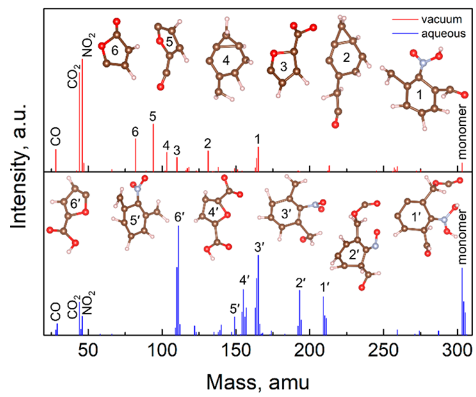

Figure 5. Distribution of reaction intermediates and products along the TDESMD trajectories for atomistic models in vacuum (red) and aqueous (blue) environments. Snapshots correspond to representative structures of abundant species along the trajectories.

peaks corresponding to species with differing number of hydrogens. Note such species (hydrogenated and dehydrogenated) are more obvious in the spectrum for the aqueous phase because of the abundant proton transfer events from/to surrounding water molecules. In the mass range of 80−105 amu, the spectrum for the vacuum phase shows features 4−6, corresponding to further cracking of dehydrogenated FDCA and nitrobenzyl fragments. These fragments are not observed in the spectrum for the aqueous phase, indicating its lower degree of degradation. In most other mass regions, the two spectra are similar, despite differences in peak intensities. Note feature 2 corresponding to a structure with a seven-membered ring and feature 4′ corresponding to $FDCA^-$ are only observed in spectra for vacuum and aqueous phases, respectively.

One has computed multiple TDESMD trajectories for atomistic models in both vacuum and aqueous environments. On the basis of that, various properties were analyzed, such as the degradation rate, duration, oscillator strength, and transition energy of each trajectory, which are shown in Supporting Information (Table S1 and Table S2). Generally, orbital pairs with high oscillator strengths are used as the initial excitation conditions for TDESMD calculations. Here, we focus on trajectories with the initial excitations of HO → LU+3 for the vacuum phase and HO-2 → LU+2 for the aqueous phase. They are the most representative trajectories showing the highest degree of degradation. The degree of degradation is estimated by numbers of fragments generated along the TDESMD trajectory. The highest degree of degradation is observed for these orbital pairs since the charge densities are localized in the same spatial region of the molecule. Such a spatial distribution is efficient for electronic excitation and de-excitation among orbital pairs, which facilitates the activation of bonds in adjacent regions. Though dissociation does occur in the aqueous phase trajectories, the higher degree of degradation of the backbone chain occurs in the vacuum phase. This could be due to kinetic energy transferred from optically excited fragments to surrounding water molecules, which provides additional channels for energy dissipation. Additionally, hydrogen bonding helps stabilize the reaction intermediates.

In the aqueous TDESMD trajectory, hydrogens actively participate in chemical reactions. It is necessary to determine the total electronic charge of involved atoms. To this end, we extract snapshots (momentary atomic positions) from the

https://doi.org/10.1021/acs.jpclett.2c00802
J. Phys. Chem. Lett. 2022, 13, 4374−4380

TDESMD trajectory and perform single point energy calculations (0 K) to obtain their electronic densities. The charges to different atoms are thus calculated based on partitioning and integration of electronic densities according to the Bader charge analysis[49−51] technique. Our results show that hydrogen transfer from/to water molecules can be considered as proton transfer reactions. For example, H with a positive charge of ∼0.6e transfers from water to the $FDCA^{2-}$ anion, leading to a carboxyl group in the $FDCA^{-}$ anion (Figure S1). Hydrogen with a positive charge of ∼0.4e transfers from the six-membered ring to water (Figure S2). On the other hand, the hydrogen transfer may be considered as hydrogen abstraction when the water molecule is not involved. From ∼2210 to ∼2230 fs, hydrogen that is connected to the sp^3-carbon transfers to the carboxylate group of the $FDCA^{-}$ anion, leading to a neutral FDCA molecule (Figure S2). Hydrogen is found with a positive charge of ∼0.1*e* at initial stages of the reaction, which is smaller than the charge of the ionized hydrogen participating in proton transfer as shown earlier. When hydrogen is ejected, one finds a positive charge of ∼0.3*e*. The charge increases since hydrogen is in proximity to the carboxylate O. Thus, without the involvement of water, labile hydrogen behaves more like a radical than a proton.

In final stages of TDESMD trajectories, a large amount of thermal energy is accumulated leading to excessive bond breaking/forming and bond elongation/contraction. To better characterize the geometries and electronic properties of products, we adopt a "cooling" strategy[25] by extracting final snapshots from TDESMD trajectories and performing structural relaxation on these snapshots to obtain ground-state structures (Figure S3). The product from the vacuum TDESMD trajectory contains closed-shell molecules CO and CO_2 as a result of degradation of the FDCA skeleton, while the product from the aqueous TDESMD trajectory contains an intact FDCA molecule. In addition, one finds the reduction of bandgaps of ∼1.5 eV and redshifts of absorption spectra for both products compared to their reactants.

In summary, photodegradation pathways of polymeric chains containing FDCA building blocks and nitrobenzyl chromophore in vacuum and aqueous environments are modeled by DFT-based TDESMD calculations with periodic boundary conditions. One finds a similar trend of photodegradation pathways for trajectories in vacuum and aqueous environments: nitro groups are labile, and the backbone chain typically breaks between the C−O bond of the alkoxy group in the linker. Molecules similar to nitrobenzene and furan are frequently observed at early stages of computed trajectories. At later stages, smaller fragments with lighter molecular weights are found, due to the accumulation of thermal energy. TDESMD trajectories in the vacuum phase show a higher degree of degradation than those in the aqueous phase. Following the breaking of polymeric chains, one observes the degradation of the FDCA backbone in the vacuum trajectory, whereas a FDCA molecule is formed and remains intact in the aqueous trajectory. Our results corroborate the recovery of the FDCA molecule from FDCA-nitrobenzyl polymer/oligomer in protonated solvents that were reported by the experiments.[5] Furthermore, our results indicate that proton transfers involving polymeric derivatives and surrounding solvent molecules are essential for the recovery of FDCA monomers. The application of TDESMD provides opportunities to investigate photoreactions for polymeric systems in various environments. Our calculations will provide insights and knowledge to explore potential energy surfaces for transition-state search, from which transition-state structures and barrier heights can be obtained for the accurate prediction of reaction yields.

■ ASSOCIATED CONTENT

Supporting Information

The Supporting Information is available free of charge at https://pubs.acs.org/doi/10.1021/acs.jpclett.2c00802.

Theoretical methods, computational details, additional degradation results from TDESMD trajectories, Bader charge analysis (PDF)

Videos of representative TDESMD trajectories (MP4-1, MP4-2)

Transparent Peer Review report available (PDF)

■ AUTHOR INFORMATION

Corresponding Authors

Bakhtiyor Rasulev − *Department of Coatings and Polymeric Materials, North Dakota State University, Fargo, North Dakota 58108, United States;* orcid.org/0000-0002-7845-4884; Email: bakhtiyor.rasulev@ndsu.edu

Dmitri Kilin − *Department of Chemistry and Biochemistry, North Dakota State University, Fargo, North Dakota 58108, United States;* orcid.org/0000-0001-7847-5549; Email: dmitri.kilin@ndsu.edu

Authors

Meade Erickson − *Department of Coatings and Polymeric Materials, North Dakota State University, Fargo, North Dakota 58108, United States*

Yulun Han − *Department of Chemistry and Biochemistry, North Dakota State University, Fargo, North Dakota 58108, United States;* orcid.org/0000-0002-8619-0233

Complete contact information is available at: https://pubs.acs.org/10.1021/acs.jpclett.2c00802

Notes

The authors declare no competing financial interest.

■ ACKNOWLEDGMENTS

This work was supported in part by the National Science Foundation through the ND EPSCoR Award #IIA-1355466. We acknowledge the use of resources at the Center for Computationally Assisted Science and Technology (CCAST) at North Dakota State University. We also thank Aaron Forde and Amirhadi Alesadi for collective discussion and editing. The authors thank the DOE BES NERSC facility for computational resources and the allocation award "Computational Modeling of Photo-catalysis and Photo-induced Charge Transfer Dynamics on Surfaces", supported by the Office of Science of the DOE under Contract DE-AC02-05CH11231. M.E. and B.R. thank the Department of Coatings and Polymeric Materials at North Dakota State University for providing the Lowell Wood funding. D.K. acknowledges the support of the National Science Foundation under Grant CHE-1944921. This work was performed, in part, at the Center for Integrated Nanotechnologies, an Office of Science User Facility operated for the U.S. Department of Energy (DOE) Office of Science by Los Alamos National Laboratory (Contract 89233218CNA000001) and Sandia National Laboratories (Contract DE-NA-0003525). D.K. thanks David Micha, Oleg

Prezhdo, Sergei Tretiak, Svetlana Kilina, Andrei Kryjevski, Benjamine Levine, Evert Jan Meijer, P. Stanley May, Mary T. Berry, and Sivaguru Jayraman for inspiring discussions.

■ REFERENCES

(1) Linthorst, J. A. An overview: origins and development of green chemistry. *Found. Chem.* **2010**, *12* (1), 55−68.

(2) Blank, L. M.; Narancic, T.; Mampel, J.; Tiso, T.; O'Connor, K. Biotechnological upcycling of plastic waste and other non-conventional feedstocks in a circular economy. *Curr. Opin. Biotechnol.* **2020**, *62*, 212−219.

(3) Li, X.; Xu, R.; Yang, J.; Nie, S.; Liu, D.; Liu, Y.; Si, C. Production of 5-hydroxymethylfurfural and levulinic acid from lignocellulosic biomass and catalytic upgradation. *Ind. Crops Prod.* **2019**, *130*, 184−197.

(4) Alam, M. I.; De, S.; Khan, T. S.; Haider, M. A.; Saha, B. Acid functionalized ionic liquid catalyzed transformation of non-food biomass into platform chemical and fuel additive. *Ind. Crops Prod.* **2018**, *123*, 629−637.

(5) Rajendran, S.; Raghunathan, R.; Hevus, I.; Krishnan, R.; Ugrinov, A.; Sibi, M. P.; Webster, D. C.; Sivaguru, J. Programmed photodegradation of polymeric/oligomeric materials derived from renewable bioresources. *Angew. Chem., Int. Ed. Engl.* **2015**, *54* (4), 1159−63.

(6) Chenoweth, K.; Cheung, S.; van Duin, A. C. T.; Goddard, W. A.; Kober, E. M. Simulations on the Thermal Decomposition of a Poly(dimethylsiloxane) Polymer Using the ReaxFF Reactive Force Field. *J. Am. Chem. Soc.* **2005**, *127*, 7192−7202.

(7) Zhao, T.; Li, T.; Xin, Z.; Zou, L.; Zhang, L. A ReaxFF-Based Molecular Dynamics Simulation of the Pyrolysis Mechanism for Polycarbonate. *Energy Fuels* **2018**, *32* (2), 2156−2162.

(8) Sai, N.; Leung, K.; Zador, J.; Henkelman, G. First principles study of photo-oxidation degradation mechanisms in P3HT for organic solar cells. *Phys. Chem. Chem. Phys.* **2014**, *16* (17), 8092−9.

(9) Han, Y.; Hobbie, E. K.; Kilin, D. S. First-Principles Molecular Dynamics of Monomethylhydrazine and Nitrogen Dioxide. *J. Phys. Chem. Lett.* **2019**, *10* (10), 2394−2399.

(10) Vogel, D. J.; Rimsza, J. M.; Nenoff, T. M. Prediction of Reactive Nitrous Acid Formation in Rare-Earth MOFs via ab initio Molecular Dynamics. *Angew. Chem., Int. Ed. Engl.* **2021**, *60* (20), 11514−11522.

(11) Meng, Q.; May, P. S.; Berry, M. T.; Kilin, D. Sequential hydrogen dissociation from a charged Pt13H24cluster modeled byab initiomolecular dynamics. *Int. J. Quantum Chem.* **2012**, *112* (24), 3896−3903.

(12) Chaban, V. V.; Prezhdo, O. V. Synergistic Amination of Graphene: Molecular Dynamics and Thermodynamics. *J. Phys. Chem. Lett.* **2015**, *6* (21), 4397−403.

(13) Chaban, V. V.; Pal, S.; Prezhdo, O. V. Laser-Induced Explosion of Nitrated Carbon Nanotubes: Nonadiabatic and Reactive Molecular Dynamics Simulations. *J. Am. Chem. Soc.* **2016**, *138* (49), 15927−15934.

(14) Disrud, B.; Han, Y.; Gifford, B. J.; Kilin, D. S. Molecular dynamics of reactions between (4,0) zigzag carbon nanotube and hydrogen peroxide under extreme conditions. *Mol. Phys.* **2018**, *116* (5−6), 708−716.

(15) Curchod, B. F. E.; Martinez, T. J. Ab Initio Nonadiabatic Quantum Molecular Dynamics. *Chem. Rev.* **2018**, *118* (7), 3305−3336.

(16) Kilina, S.; Kilin, D.; Tretiak, S. Light-Driven and Phonon-Assisted Dynamics in Organic and Semiconductor Nanostructures. *Chem. Rev.* **2015**, *115* (12), 5929−78.

(17) Nelson, T.; Fernandez-Alberti, S.; Chernyak, V.; Roitberg, A. E.; Tretiak, S. Nonadiabatic excited-state molecular dynamics: numerical tests of convergence and parameters. *J. Chem. Phys.* **2012**, *136* (5), 054108.

(18) Nelson, T.; Fernandez-Alberti, S.; Roitberg, A. E.; Tretiak, S. Nonadiabatic excited-state molecular dynamics: modeling photophysics in organic conjugated materials. *Acc. Chem. Res.* **2014**, *47* (4), 1155−64.

(19) Nelson, T. R.; White, A. J.; Bjorgaard, J. A.; Sifain, A. E.; Zhang, Y.; Nebgen, B.; Fernandez-Alberti, S.; Mozyrsky, D.; Roitberg, A. E.; Tretiak, S. Non-adiabatic Excited-State Molecular Dynamics: Theory and Applications for Modeling Photophysics in Extended Molecular Materials. *Chem. Rev.* **2020**, *120* (4), 2215−2287.

(20) Tapavicza, E.; Bellchambers, G. D.; Vincent, J. C.; Furche, F. Ab initio non-adiabatic molecular dynamics. *Phys. Chem. Chem. Phys.* **2013**, *15* (42), 18336−48.

(21) Tully, J. Molecular dynamics with electronic transitions. *J. Chem. Phys.* **1990**, *93* (2), 1061.

(22) Vincent, J. C.; Muuronen, M.; Pearce, K. C.; Mohanam, L. N.; Tapavicza, E.; Furche, F. That Little Extra Kick: Nonadiabatic Effects in Acetaldehyde Photodissociation. *J. Phys. Chem. Lett.* **2016**, *7* (20), 4185−4190.

(23) Sifain, A. E.; Bjorgaard, J. A.; Nelson, T. R.; Nebgen, B. T.; White, A. J.; Gifford, B. J.; Gao, D. W.; Prezhdo, O. V.; Fernandez-Alberti, S.; Roitberg, A. E.; et al. Photoexcited Nonadiabatic Dynamics of Solvated Push-Pull pi-Conjugated Oligomers with the NEXMD Software. *J. Chem. Theory Comput.* **2018**, *14* (8), 3955−3966.

(24) Han, Y.; Meng, Q.; Rasulev, B.; May, P. S.; Berry, M. T.; Kilin, D. S. Photofragmentation of the Gas-Phase Lanthanum Isopropylcyclopentadienyl Complex: Computational Modeling vs Experiment. *J. Phys. Chem. A* **2015**, *119* (44), 10838−48.

(25) Han, Y.; Meng, Q.; Rasulev, B.; May, P. S.; Berry, M. T.; Kilin, D. S. Photoinduced Charge Transfer versus Fragmentation Pathways in Lanthanum Cyclopentadienyl Complexes. *J. Chem. Theory Comput.* **2017**, *13* (9), 4281−4296.

(26) Rabi, I. I. Space Quantization in a Gyrating Magnetic Field. *Phys. Rev.* **1937**, *51* (8), 652−654.

(27) Rabi, I. I.; Ramsey, N. F.; Schwinger, J. Use of Rotating Coordinates in Magnetic Resonance Problems. *Rev. Mod. Phys.* **1954**, *26* (2), 167−171.

(28) Han, Y.; Rasulev, B.; Kilin, D. S. Photofragmentation of Tetranitromethane: Spin-Unrestricted Time-Dependent Excited-State Molecular Dynamics. *J. Phys. Chem. Lett.* **2017**, *8* (14), 3185−3192.

(29) Han, Y.; Anderson, K.; Hobbie, E. K.; Boudjouk, P.; Kilin, D. S. Unraveling Photodimerization of Cyclohexasilane from Molecular Dynamics Studies. *J. Phys. Chem. Lett.* **2018**, *9* (15), 4349−4354.

(30) Han, Y.; Kilin, D. S.; May, P. S.; Berry, M. T.; Meng, Q. Photofragmentation Pathways for Gas-Phase Lanthanide Tris-(isopropylcyclopentadienyl) Complexes. *Organometallics* **2016**, *35* (20), 3461−3473.

(31) Disrud, B.; Han, Y.; Kilin, D. S. Molecular dynamics of laser-assisted decomposition of unstable molecules at the surface of carbon nanotubes: case study of CH2(NO2)2 on CNT(4,0). *Mol. Phys.* **2017**, *115* (5), 674−682.

(32) Chen, J.; Meng, Q.; Stanley May, P.; Berry, M. T.; Kilin, D. S. Time-dependent excited-state molecular dynamics of photodissociation of lanthanide complexes for laser-assisted metal-organic chemical vapour deposition. *Mol. Phys.* **2014**, *112* (3−4), 508−517.

(33) Perdew, J. P.; Burke, K.; Ernzerhof, M. Generalized Gradient Approximation Made Simple. *Phys. Rev. Lett.* **1996**, *77* (18), 3865−3868.

(34) Perdew, J. P.; Burke, K.; Ernzerhof, M. Generalized Gradient Approximation Made Simple. *Phys. Rev. Lett.* **1996**, *77* (18), 3865−3868.

(35) Perdew, J. P.; Chevary, J. A.; Vosko, S. H.; Jackson, K. A.; Pederson, M. R.; Singh, D. J.; Fiolhais, C. Atoms, Molecules, Solids, and Surfaces: Applications of the Generalized Gradient Approximation for Exchange and Correlation. *Phys. Rev. B* **1992**, *46* (11), 6671−6687.

(36) Blöchl, P. E. Projector augmented-wave method. *Phys. Rev. B* **1994**, *50* (24), 17953−17979.

(37) Kohn, W.; Sham, L. J. Self-Consistent Equations Including Exchange and Correlation Effects. *Phys. Rev.* **1965**, *140* (4A), A1133−A1138.

(38) Kresse, G.; Hafner, J. Ab initio molecular dynamics for liquid metals. *Phys. Rev. B: Condens. Matter Mater. Phys.* **1993**, *47* (1), 558−561.
(39) Kresse, G.; Hafner, J. Ab initio molecular-dynamics simulation of the liquid-metal-amorphous-semiconductor transition in germanium. *Phys. Rev. B: Condens. Matter Mater. Phys.* **1994**, *49* (20), 14251−14269.
(40) Kresse, G.; Furthmuller, J. Efficient iterative schemes for ab initio total-energy calculations using a plane-wave basis set. *Phys. Rev. B* **1996**, *54*, 11169−11186.
(41) Kresse, G.; Furthmuller, J. Efficiency of ab-initio total energy calculations for metals and semiconductors using a plane-wave basis set. *Comput. Mater. Sci.* **1996**, *6*, 15−50.
(42) Grimme, S.; Antony, J.; Ehrlich, S.; Krieg, H. A consistent and accurate ab initio parametrization of density functional dispersion correction (DFT-D) for the 94 elements H-Pu. *J. Chem. Phys.* **2010**, *132* (15), 154104.
(43) O'Boyle, N. M; Banck, M.; James, C. A; Morley, C.; Vandermeersch, T.; Hutchison, G. R Open Babel: An open chemical toolbox. *J. Cheminformatics* **2011**, *3*, 33.
(44) Forde, A.; Inerbaev, T.; Hobbie, E. K.; Kilin, D. S. Excited-State Dynamics of a CsPbBr3 Nanocrystal Terminated with Binary Ligands: Sparse Density of States with Giant Spin-Orbit Coupling Suppresses Carrier Cooling. *J. Am. Chem. Soc.* **2019**, *141* (10), 4388−4397.
(45) Vogel, D. J.; Kilin, D. S. First-Principles Treatment of Photoluminescence in Semiconductors. *J. Phys. Chem. C* **2015**, *119* (50), 27954−27964.
(46) Gaplovsky, M.; Il'ichev, Y. V.; Kamdzhilov, Y.; Kombarova, S. V.; Mac, M.; Schworer, M. A.; Wirz, J. Photochemical reaction mechanisms of 2-nitrobenzyl compounds: 2-nitrobenzyl alcohols form 2-nitroso hydrates by dual proton transfer. *Photochem. Photobiol. Sci.* **2005**, *4* (1), 33−42.
(47) Klan, P.; Solomek, T.; Bochet, C. G.; Blanc, A.; Givens, R.; Rubina, M.; Popik, V.; Kostikov, A.; Wirz, J. Photoremovable protecting groups in chemistry and biology: reaction mechanisms and efficacy. *Chem. Rev.* **2013**, *113* (1), 119−191.
(48) Patchornik, A.; Amit, B.; Woodward, R. B. Photosensitive Protecting Groups. *J. Am. Chem. Soc.* **1970**, *92*, 6333−6335.
(49) Tang, W.; Sanville, E.; Henkelman, G. A grid-based Bader analysis algorithm without lattice bias. *J. Phys.: Condens. Matter* **2009**, *21* (8), 084204.
(50) Sanville, E.; Kenny, S. D.; Smith, R.; Henkelman, G. Improved grid-based algorithm for Bader charge allocation. *J. Comput. Chem.* **2007**, *28* (5), 899−908.
(51) Henkelman, G.; Arnaldsson, A.; Jónsson, H. A fast and robust algorithm for Bader decomposition of charge density. *Comput. Mater. Sci.* **2006**, *36* (3), 354−360.

https://doi.org/10.1021/acs.jpclett.2c00802
J. Phys. Chem. Lett. 2022, 13, 4374−4380